Efficient FDTD Modeling of Irises/Slots in Microwave Structures and Its Application to the Design of Combline Filters

Ao Sheng Rong, *Member, IEEE,* Heng Yang, Xing Hao Chen, and Andreas Cangellaris, *Fellow, IEEE*

***Abstract*—A new methodology is proposed for the computationally efficient, numerically stable, and accurate finite difference time-domain (FDTD) simulation of microwave structures with electrically thin irises and slots. The proposed method is based on the hybridization of Yee's standard FDTD scheme with Pad,é approximations of the electromagnetic properties of the irises/slots. Through the use of rigorous modal expansions for the description of the fields in the waveguide sections formed by the irises and slots, highly accurate rational function approximations of their transmission and reflection properties are obtained. These transfer functions are then incorporated directly in the FDTD algorithm through their corresponding z-transform expressions. Combined with the matrix valued multivariate Padé approximation, the proposed method provides a suitable design tool for combline filters and manifold multiplexes for satellite and wireless communication systems. Results are presented to demonstrate the validity and accuracy of the proposed methodology.**

***Index Terms*—Microwave circuits, rational approximation, time- domain analysis.**

I. Introduction

COMBLINE filters and multiplexes used in satellite and wireless communications systems often involve irises or slots to effect electromagnetic coupling between adjacent or nonadjacent cavities [1]–[3]. In printed antennas [4], patches are usually slot-coupled with feed lines. The MMIC compatible microstrip-to-waveguide transition is another example of slot couplings [5]. In three-dimensional (3-D_, multichip-module (MCM) interconnects [6], traces on different layers are often connected to each other by vias through perforated ground planes. In all the aforementioned applications, the irises or slots are electrically small in one or more dimensions. Thus, for their accurate numerical modeling, techniques such as the finite difference time-domain (FDTD) method [7]–[12] require the implementation of special grid refinement techniques in the neighborhood of the irises and slots. These techniques include subgridding (either global or locally conformal), specialized equations derived through finite-volume integrations, etc.

An alternative methodology to handle such irises and slots is presented in this paper. The coupling irises and slots are modeled as sections of uniform waveguides. Thus, their electromagnetic fields are approximated in terms of a finite set of eigenmodes. At the interface between irises/slots and their adjacent regions, continuity of the tangential electric and magnetic fields is enforced through impedance relations that involve the waveguide modal impedances. Since the modal impedances are available in closed form, their higher order derivatives with respect to the complex frequency $s = j\omega$ can be obtained analytically. Thus, Padé approximation techniques can be used to cast the aforementioned impedance relations in terms of rational functions of s. Subsequently, application of the z transform leads to FDTD-compatible expressions for the impedance relationships between the transverse electric and magnetic fields at the interfaces between the iris/slot and the adjacent domains.

Because FDTD is typically computation-intensive, its brute-force integration with optimization strategies for the computer-aided design (CAD) of microwave passive components, such as filters and multiplexes, is computationally cumbersome and often times prohibitive, even beyond the capabilities of today's ordinary workstations. To address this shortcoming, this paper considers also the use of matrix-valued multivariate Padé approximation as a means to obtain closed-form expressions for the FDTD-generated scattering matrix elements for a given device, obtained at a set of sampling points in a multidimensional space, for subsequent use for device optimization. More specifically, the generalized inverse rational interpolants (GIRIs) algorithm [13], [14] is enhanced to yield a novel algorithm, called recursive GIRIs, to be used for this purpose.

The mathematical details of the development of the proposed rigorous model for slots and irises are presented in Section II. This is followed by the description of the use of the matrix-valued multivariate Padé approximation, along with the development and implementation of the recursive GIRIs algorithm in Section III. In Section IV, examples are presented from the application of the generated models to the FDTD analysis of typical building blocks in combline filters and multiplexers. Section V presents examples from the application of the proposed methodologies to the design and optimization of coupling between waveguides and resonators, as well as its use in the design of 900- and 1800-MHz combline filters.

Manuscript received March 29, 2001; revised August 18, 2001.

A. S. Rong is with the Department of Electrical and Computer Engineering, University of Illinois at Urbana-Champaign, Urbana, IL 61801 USA and also with the State Key Laboratory of Millimeter Waves, Department of Radio Engineering, Southeast University, Nanjing 210096, China.

H. Yang and X. H. Chen are with the State Key Laboratory of Millimeter Waves, Department of Radio Engineering, Southeast University, Nanjing 210096, China.

A. Cangellaris is with the Department of Electrical and Computer Engineering, University of Illinois at Urbana-Champaign, Urbana, IL 61801 USA.

Publisher Item Identifier S 0018-9480(01)10469-2.

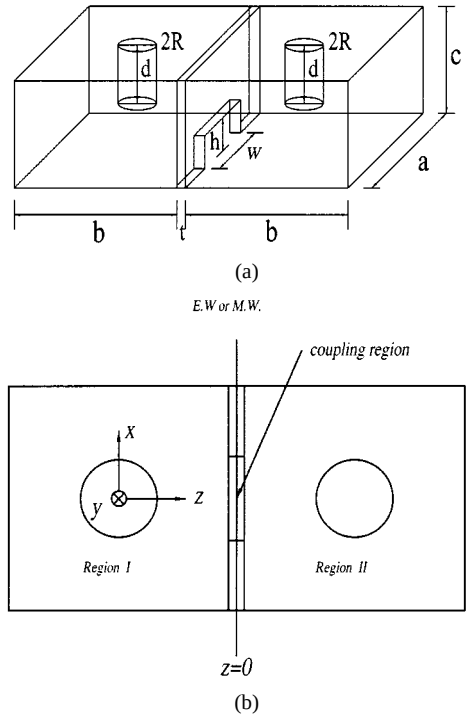

Fig. 1. Slot-coupled rectangular combline resonators. (a) Perspective view of the structure. (b) Top view. For the symmetric structure shown, an electric wall (E.W.) or a magnetic wall (M.W.) is used to extract the two-port impedance relationships.

II. Development of the FDTD-Compatible Models

For the sake of clarity, the slot-coupled rectangular combline resonators shown in Fig. 1, a typical building block in high-Q filters and multiplexes in wireless communications, are used to demonstrate the development of the proposed models. However, the methodology is general and can be extended easily to a variety of other related structures.

With reference to Fig. 1(b), the coupling slot is modeled as a section of a homogeneous, uniform waveguide of permittivity ε and permeability μ. Thus, the transverse (to z) electromagnetic fields in the slot can be written as [15], [16]

$$\mathbf{E}_t = \sum_m V_m^h(z)\mathbf{e}_m^h(x,\,y) + \sum_n V_n^e(z)\mathbf{e}_n^e(x,\,y) \quad (1a)$$

$$\mathbf{H}_t = \sum_m I_m^h(z)\mathbf{h}_m^h(x,\,y) + \sum_n I_n^e(z)\mathbf{h}_n^e(x,\,y) \quad (1b)$$

where $\mathbf{e}_i(x,\,y)$ and $\mathbf{h}_i(x,\,y)$ satisfy the relation

$$\mathbf{h}_i(x,\,y) = \mathbf{u}_z \times \mathbf{e}_i(x,\,y).$$

When symmetry is used, the transverse electromagnetic fields at the interface between the slot and the combline resonator can be related to each other with

$$\mathbf{E}_t = \sum_m Z_m^h(s)\mathbf{e}_m^h(x,\,y)\iint_{slot}\mathbf{H}_t \bullet \mathbf{h}_m^h(x,\,y)\,ds + \sum_n Z_n^e(s)\mathbf{e}_n^e(x,\,y)\iint_{slot}\mathbf{H}_t \bullet \mathbf{h}_n^e(x,\,y)\,ds \quad (2)$$

where $Z_m^h(s)$ and $Z_n^e(s)$ have analytical expressions in the s domain as follows:

$$Z_m^h(s) = \frac{s\mu}{\sqrt{\varepsilon\mu s^2 + K_{cm}^2}}\tanh\left(\frac{t}{2}\sqrt{\varepsilon\mu s^2 + K_{cm}^2}\right)$$
$$Z_n^e(s) = \frac{\sqrt{\varepsilon\mu s^2 + K_{cn}^2}}{s\varepsilon}\tanh\left(\frac{t}{2}\sqrt{\varepsilon\mu s^2 + K_{cn}^2}\right) \quad (3a)$$

for perfect electric wall at the plane of symmetry and

$$Z_m^h(s) = \frac{s\mu}{\sqrt{\varepsilon\mu s^2 + K_{cm}^2}}\coth\left(\frac{t}{2}\sqrt{\varepsilon\mu s^2 + K_{cm}^2}\right)$$
$$Z_n^e(s) = \frac{\sqrt{\varepsilon\mu s^2 + K_{cn}^2}}{s\varepsilon}\coth\left(\frac{t}{2}\sqrt{\varepsilon\mu s^2 + K_{cn}^2}\right) \quad (3b)$$

for perfect magnetic wall at the plane of symmetry. In the above expressions, K_{cm} and K_{cn} represent the cutoff wavenumbers. For the regular cross section, such as rectangular or circular, simple closed-form expressions are available for the cutoff wavenumbers. However, for the general case of irregular cross section, calculation of K_{cm} and K_{cn} requires a numerical two-dimensional (2-D) eigensolver.

For asymmetrical structures, $\mathbf{E}_{ti}$ and $\mathbf{H}_{ti}$ on the two sides of the coupling slot are related to each other through a block-diagonal modal impedance matrix as follows:

$$\begin{aligned}\mathbf{E}_{t1} = {} & \sum_m Z_{m11}^h(s)\mathbf{e}_m^h(x,\,y)\iint_{slot}\mathbf{H}_{t1} \bullet \mathbf{h}_m^h(x,\,y)\,ds \\ & + \sum_n Z_{n11}^e(s)\mathbf{e}_n^e(x,\,y)\iint_{slot}\mathbf{H}_{t1} \bullet \mathbf{h}_n^e(x,\,y)\,ds \\ & + \sum_m Z_{m12}^h(s)\mathbf{e}_m^h(x,\,y)\iint_{slot}\mathbf{H}_{t2} \bullet \mathbf{h}_m^h(x,\,y)\,ds \\ & + \sum_n Z_{n12}^e(s)\mathbf{e}_n^e(x,\,y)\iint_{slot}\mathbf{H}_{t2} \bullet \mathbf{h}_n^e(x,\,y)\,ds \end{aligned} \quad (4a)$$

$$\begin{aligned}\mathbf{E}_{t2} = {} & \sum_m Z_{m21}^h(s)\mathbf{e}_m^h(x,\,y)\iint_{slot}\mathbf{H}_{t1} \bullet \mathbf{h}_m^h(x,\,y)\,ds \\ & + \sum_n Z_{n21}^e(s)\mathbf{e}_n^e(x,\,y)\iint_{slot}\mathbf{H}_{t1} \bullet \mathbf{h}_n^e(x,\,y)\,ds \\ & + \sum_m Z_{m22}^h(s)\mathbf{e}_m^h(x,\,y)\iint_{slot}\mathbf{H}_{t2} \bullet \mathbf{h}_m^h(x,\,y)\,ds \\ & + \sum_n Z_{n22}^e(s)\mathbf{e}_n^e(x,\,y)\iint_{slot}\mathbf{H}_{t2} \bullet \mathbf{h}_n^e(x,\,y)\,ds. \end{aligned} \quad (4b)$$

The nonzero elements of the block-diagonal modal impedance matrix are available in closed form as

$$\begin{aligned} Z_{m11}^h(s) &= Z_{m22}^h(s) \\ &= \frac{s\mu}{\sqrt{\varepsilon\mu s^2 + K_{cm}^2}}\coth\left(t\sqrt{\varepsilon\mu s^2 + K_{cm}^2}\right) \\ Z_{n11}^e(s) &= Z_{n22}^e(s) \\ &= \frac{\sqrt{\varepsilon\mu s^2 + K_{cn}^2}}{s\varepsilon}\coth\left(t\sqrt{\varepsilon\mu s^2 + K_{cn}^2}\right) \end{aligned} \quad (5a)$$

$$Z^h_{m12}(s) = Z^h_{m21}(s) = \frac{s\mu}{\sqrt{\varepsilon\mu s^2 + K^2_{cm}}} \cdot \frac{1}{\sinh\left(t\sqrt{\varepsilon\mu s^2 + K^2_{cm}}\right)}$$
$$Z^e_{n12}(s) = Z^e_{n21}(s) = \frac{\sqrt{\varepsilon\mu s^2 + K^2_{cn}}}{s\varepsilon} \cdot \frac{1}{\sinh\left(t\sqrt{\varepsilon\mu s^2 + K^2_{cn}}\right)}. \quad (5b)$$

To create the update scheme for $\mathbf{E}_t$ at the interface, it is necessary for (2) or (4) to be cast in a time-dependent form compatible with the FDTD scheme. Toward this objective, $Z^h_m(s)$ and $Z^e_n(s)$ are expanded in terms of Taylor series as follows:

$$Z(s) = z_0 + z_1 s + z_2 s^2 + z_3 s^3 + \cdots \quad (6)$$

where the expansion coefficients, z_i, are easily generated, due to the available analytical expressions for $Z^h_m(s)$ and $Z^e_n(s)$ [see (3) and (5)]. Subsequently, rational function approximations for $Z^h_m(s)$ and $Z^e_n(s)$ are introduced. They are of the form

$$Z(s) = \frac{a_0 + a_1 s + a_2 s^2 + \cdots + a_L s^L}{b_0 + b_1 s + b_2 s^2 + \cdots + b_M s^M} \quad (7)$$

and their coefficients are deduced from (6) using the Padé approximation [17]. With $b_0 = 1$, following the standard procedure of the Padé approximation, the coefficients of the denominator are derived as the solution to the system

$$\begin{bmatrix} z_{L-M+1} & z_{L-M+2} & \cdots & z_L \\ z_{L-M+2} & z_{L-M+3} & \cdots & z_{L+1} \\ \vdots & \vdots & \vdots & \vdots \\ z_L & z_{L+1} & \cdots & z_{L+M-1} \end{bmatrix} \begin{bmatrix} b_M \\ b_{M-1} \\ \vdots \\ b_1 \end{bmatrix} = - \begin{bmatrix} z_{L+1} \\ z_{L+2} \\ \vdots \\ z_{L+M} \end{bmatrix}. \quad (8)$$

Subsequently, the numerator coefficients are obtained by setting (6) equal to (7); this yields the matrix equation

$$\begin{bmatrix} z_0 & 0 & 0 & \cdots & 0 \\ z_1 & z_0 & 0 & \cdots & 0 \\ & & \cdots & & \\ z_L & z_{L-1} & z_{L-2} & \cdots & z_{L-M} \end{bmatrix} \begin{bmatrix} b_0 \\ b_1 \\ \vdots \\ b_M \end{bmatrix} = \begin{bmatrix} a_0 \\ a_1 \\ \vdots \\ a_L \end{bmatrix}. \quad (9)$$

Once the Padé approximations for $Z^h_m(s)$ and $Z^e_n(s)$ have been generated, their z-domain forms

$$Z(z) = \frac{c_0 + c_1 z^{-1} + c_2 z^{-2} + \cdots + c_m z^{-m}}{d_0 + d_1 z^{-1} + d_2 z^{-2} + \cdots + d_n z^{-n}} \quad (10)$$

are obtained through the bilinear transformation [18], [19]

$$s = \frac{2}{\Delta t} \times \frac{1 - z^{-1}}{1 + z^{-1}}. \quad (11)$$

In (11) Δt is equal to the time step in the FDTD algorithm. Substitution of these z-domain expressions for $Z^h_m(s)$ and $Z^e_n(s)$ in (2) or (4) yield difference equations for updating $\mathbf{E}_t$ at the two end surfaces of the coupling iris or slot. Taking into account the one-half time step shift between $\mathbf{E}_t$ and $\mathbf{H}_t$, the actual update value for $\mathbf{E}_t$ is adjusted to be the average over one time step as follows:

$$\mathbf{E}_t = \mathbf{E}_t \left(\frac{1 + z^{-1}}{2}\right). \quad (12)$$

This step completes the development of the FDTD-compatible, rigorous model for electromagnetic coupling between two regions through slots and irises.

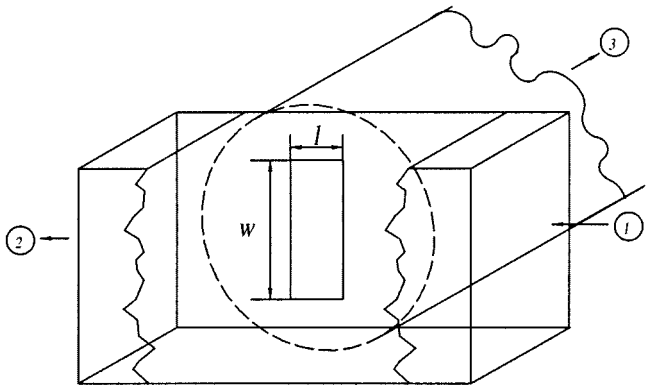

Fig. 2. Geometry of a T-junction between a rectangular and a circular waveguide utilizing a rectangular slot for the coupling.

III. Matrix-Valued Mutlivariable Padé Approximation

In this section, the process used to facilitate and expedite the design and optimization of microwave components through FDTD-assisted modeling is presented. For this purpose, the coupling through the slot in the T-junction geometry of Fig. 2 will be used as the demonstration vehicle. This coupling structure between a rectangular waveguide with a circular one constitutes a key building block in manifold multiplexes. The rectangular waveguide is the common path for the RF signals. The purpose of the rectangular coupling slot is two-fold. First, it is used to realize the coupling of RF signals between the R/F ends and the channel filters and, second, it contributes to the impedance transform required for the design of dual-mode filters. Often times the coupling slot may have rounded corners or be elliptic in shape.

When the FDTD-compatible model described in the previous section is used to analyze this T-junction, the quantities of interest are the elements of the scattering-parameter matrix for the dominant mode

$$S = \begin{pmatrix} S_{11} & S_{12} & S_{13} \\ S_{21} & S_{22} & S_{23} \\ S_{31} & S_{32} & S_{33} \end{pmatrix} \quad (13)$$

where S_{ij} is a function of the frequency and the structural parameters. In design optimization of multiplexes, the optimization parameters are the frequency f, the length w, and width l of the slot, while the cross-sectional dimensions of the rectangular waveguide, the radius of the circular waveguide, and the thickness of the slot are supposed to be kept constant. Brute-force application of the FDTD algorithm to the optimization of the

design through a trial and error process is cumbersome and time consuming. An effective alternative is the development of closed-form expressions for the scattering parameters as functions of frequency and the length and width of the slot. To this end, the complex matrix valued multivariable Padé approximation will be used.

The complex matrix valued Padé approximation algorithm for the single-variable case is considered first. The proposed algorithm is an extension of the GIRI's algorithm for vector valued rational interpolants proposed by Graves-Morris [13], [14]. The description of the algorithm is given below.

Given a set of sampling points $\{x_i,\ i = 0, 1, 2, \ldots, n: x_i \in \boldsymbol{R}\}$ and a set of complex matrices $\{\boldsymbol{A}^{(i)},\ i = 0, 1, 2, \ldots, n: \mathbf{A}^{(i)} \in \boldsymbol{C}^{d\times d}\}$, each complex matrix $\mathbf{A}^{(i)}$ is associated with a distinct real sampling point x_i. A matrix $\mathbf{S}$ in $\boldsymbol{C}^{d\times d}$ can be interpolated by a rational function as

$$\mathbf{S}(x) = \mathbf{N}(x)/D(x) \tag{14}$$

where $\mathbf{N}(x)$ is a $d \times d$-dimensional matrix of polynomials and $D(x)$ is a polynomial. The construction process (GIRI's algorithm) is as follows:

Step 1: *Initialization*. Define

$$\mathbf{B}^{(0)} = \mathbf{A}^{(0)} \tag{15}$$

and, for $i = 1, 2, \ldots, n$,

$$\mathbf{S}^{(1)}(x_i) = \frac{x_i - x_0}{\mathbf{A}^{(i)} - \mathbf{B}^{(0)}}. \tag{16}$$

Step 2: *Iteration.*For $k = 1, 2, \ldots, n-1$, define

$$\mathbf{B}^{(k)} = \mathbf{S}^{(k)}(x_k) \tag{17}$$

and, for $i = k+1, k+2, \ldots, n$,

$$\mathbf{S}^{(k+1)}(x_i) = \frac{x_i - x_k}{\mathbf{S}^{(k)}(x_i) - \mathbf{B}^{(k)}}. \tag{18}$$

Step 3: *Termination*. Define

$$\mathbf{B}^{(n)} = \mathbf{S}^{(n)}(x_n). \tag{19}$$

The resulting construct is

$$\mathbf{S}(x) = \mathbf{B}^{(0)} + \frac{x - x_0}{\mathbf{B}^{(1)}} + \frac{x - x_1}{\mathbf{B}^{(2)}} + \cdots + \frac{x - x_{n-1}}{\mathbf{B}^{(n)}}. \tag{20}$$

By the tail-to-head rationalization, it turns out that $\mathbf{S}(x)$ is of the form in (14) where $\mathbf{B}^{-1}$ is the Samelson inverse of $\mathbf{B}$ and is defined as

$$B^{-1} = B^*/\|B\|^2, \qquad \|B\|^2 = \sum_i \sum_j |b_{ij}|^2. \tag{21}$$

For the multivariable case, an algorithm is devised for the recursive construction of the matrix Padé approximation through a repeated use of the aforementioned single-variable algorithm. Let $\mathcal{H}^n$ be a given set of n variables with γ sampling points. For an arbitrary point $\overline{x}^*$, the matrix value $\mathbf{S}$ at the point $\overline{x}^*$ is interpolated as $S(\overline{x}^*) = \hat{S}(\overline{x}^*)$, where $\hat{\mathbf{S}}$ is a matrix of rational functions calculated in the following manner. The set $\mathcal{H}^n$ is split into two subsets, $\mathcal{H}^1$ and $\mathcal{H}^{n-1}$. $\mathcal{H}^1$ consists of the sampling frequency points and $\mathcal{H}^{n-1}$ is a set of the sampling structural parameters. If necessary, $\mathcal{H}^{n-1}$ can be further split into subsets. For example, for the case of the T-junction under consideration $\mathcal{H}^{n-1}$ is equal to $\{(w_i, l_i)|(w_i, l_i) \in R^2\}$. In $\mathcal{H}^1$, the approximant is obtained directly using the single-valued GIRI's algorithm. In $\mathcal{H}^{n-1}$, the approximant is derived by a recursive application of GIRI's algorithm for the single-variable case using the recursive procedure of [20]. Finally, the approximant for $\hat{\mathbf{S}}$ is found by a recursive application of the approximants in $\mathcal{H}^1$ and $\mathcal{H}^{n-1}$. This completes the matrix valued multivariable Padé approximation.

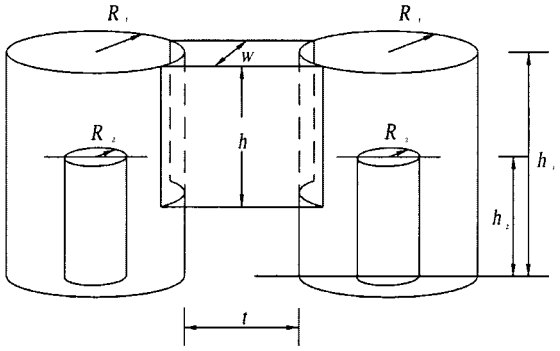

Fig. 3. Slot-coupled cylindrical combline resonators.

IV. Verification of the Proposed Model

In order to validate the proposed FDTD-compatible, broadband electromagnetic model for coupling slots and irises, the combline resonator structures shown in Figs. 1 and 3 were analyzed. The coupling coefficient is calculated from the two resonant frequencies f_e for the electric wall case and f_m for the magnetic wall case through the expression $(f_m^2 - f_e^2)/(f_m^2 + f_e^2)$. f_e and f_m are further obtained using the fast Fourier transform (FFT)/Padé approximation as described below.

It is well known that, when the temporal response of the FDTD simulation is transformed to the frequency domain, say, via FFT, the frequency resolution is of the order of $\Delta f \sim 1/N\Delta t$, and its accuracy may not be sufficient for highly precise calculation of the aforementioned resonant frequencies. To address this obstacle, the combination of the Padé approximation with FFT is proposed to calculate f_e and f_m. The spectrum of the FDTD generated temporal data is computed first via FFT. Subsequently, a rational function is constructed to fit the spectral response. The rational function is obtained directly using the singular value decomposition (SVD) of a data matrix [21]. The SVD allows one to estimate the required order of the polynomials in the denominator and numerator of the approximation model. The coefficients of the polynomials are obtained using the method of total least squares (TLS). This construction of the rational function has the following two significant advantages: 1) the suppression of the effects of noise in FDTD spectral data and 2) the avoidance of spurious roots in the high-order rational functions. This way, the resonant frequency is actually one of the points at which the derivative of the rational function is zero. Thus, the resonant frequency is easily calculated using a polynomial root-searching program, for the polynomial obtained when the first-order derivative of the rational function is set to zero.

Fig. 4 depicts the dependence of electromagnetic coupling on the relative slot height $(c - h)/c$ with the slot thickness t as a parameter. It is observed that the slot height changes the electromagnetic property of the couplings. When the slot height is

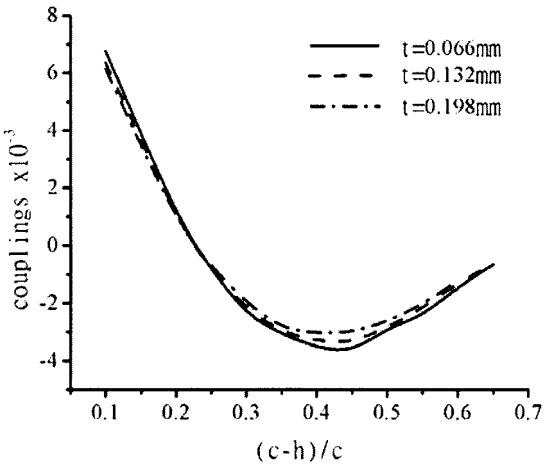

Fig. 4. Electromagnetic coupling for the slot-coupled rectangular resonators versus the relative slot height (c − h)/c, with the slot thickness t as a parameter. $a = 2.22$ mm, $b = 2.54$ mm, $c = 4.75$ mm, $R = 0.33$ mm, $d = 2.75$ mm, and $w = 2.22$ mm.

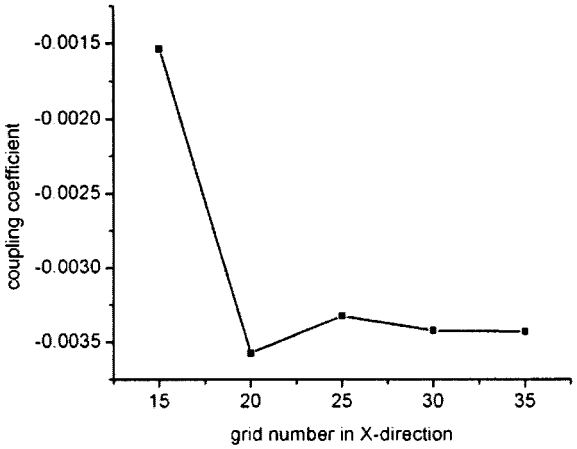

(a)

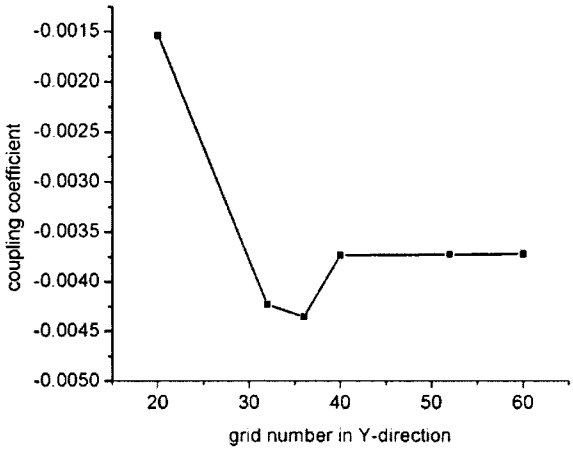

(b)

Fig. 5. Dependence of the coupling coefficient on the number of grid points for the structure of Fig. 1 in: (a) the x- and (b) y-directions.

large, the magnetic coupling becomes dominant. In the opposite case, the electric coupling becomes strong. However, the electric coupling is not a monotonic function of height. On the other hand, both electric and magnetic couplings decrease with the thickness of the slot. Depending on the properties of the elements in the coupling matrix, both electrical and magnetic couplings are required in the design of combline filters.

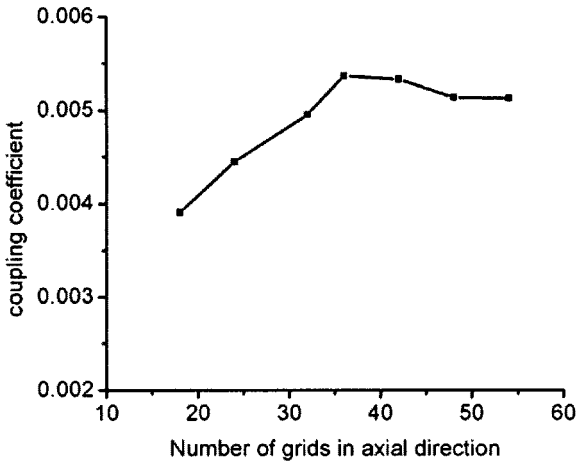

(a)

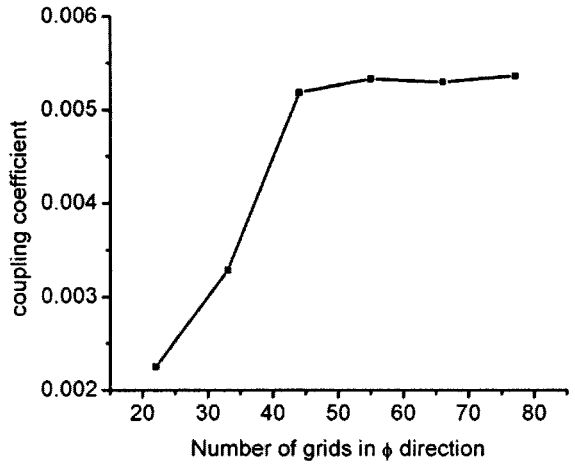

(b)

Fig. 6. Dependence of the coupling coefficient on the number of the FDTD grid points for the case of a circular combline resonator in the: (a) axial and (b) ϕ directions.

In order to examine the dependence of the modeling accuracy on the number of FDTD grid cells required over the cross section of the slot/iris, the value of the calculated coupling coefficient was plotted in Figs. 5 and 6 for the slot-coupled rectangular and cylindrical combline resonators, respectively.

Fig. 7 depicts the effect of the slot height on the coupling for the slot-coupled cylindrical combline resonators, with the slot thickness as a parameter. Also shown in this figure are experimental data obtained from [3]. Very good agreement is observed between the experimental data and the simulation results.

V. Design of Combline Filters and T-Junctions

In this section, the matrix-valued, multivariable Padé approximation discussed in Section III is used to generate closed-form expression for the scattering parameters for combline filters and T-junctions with the frequency and the desired structural dimensions as independent variables. The availability of such closed-form expressions enables expedient design optimization of the aforementioned structures.

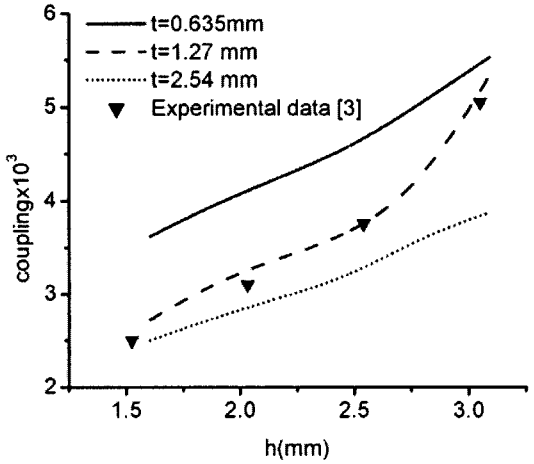

Fig. 7. Effect of the slot height on the coupling coefficients for the slot-coupled circular combline resonators, with the slot thickness as a parameter. $R_1 = 1.901$ mm, $R_2 = 0.556$ mm, $h_1 = 4.638$ mm, $h_2 = 4.389$ mm, and $w = 2.032$ mm.

A. T-Junction Slot Coupled to a Circular Waveguide

The first application is the T-junction shown in Fig. 3. The rectangular waveguide is nonstandard BJ-220 with dimensions of 10.7×4.33 mm^2. The radius of the circular waveguide is 17 mm. The thickness of the coupling slot is 0.5 mm. The sample space $\mathcal{H}^3$ is a set of three parameters (two for the dimensions of the slot and one for the frequency) with $8 \times 8 \times 12$ sample points. In accordance with the configuration space of the T-junction required for practical Ku-band channel dual-mode filters and multiplexes, the slot length w falls in the interval 5 mm $\leq w \leq 7$ mm, while for the slot width l it is 1 mm $\leq l \leq 2$ mm.

FDTD simulation is performed to create a database for the dominant-mode scattering matrix $\mathbf{S}$ at the sample points. The matrix-valued multivariable Padé approximation algorithm described above is used to generate the closed-form scattering matrix rational function with the aforementioned three parameters as independent variables. Fig. 8(a) and (b) provides the comparison between the fitted scattering parameters to those calculated through the application of the FDTD algorithm for a large number of frequencies over the desired bandwidth. Excellent agreement is observed indicating the accuracy and effectiveness of the matrix valued multivariable Padé approximation.

To further examine the validity of the generated closed-form scattering matrix rational function, the reflection coefficient at port 1 and the transmission coefficient from port 1 to port 2, with port 3 (at the circular waveguide) shorted at a distance d from the slot, was calculated. In Fig. 9, the magnitudes of the reflection and transmission coefficients calculated from the fitted model are compared to measured results and to results obtained through brute-force FDTD simulation over the bandwidth of interest. In FDTD simulation, PML absorbing boundary conditions with the optimized conductivity profile [22] are used to terminate input/output ports. As indicated in (2) and (4), on the coupling slots, the couplings of transverse electric fields are computed via integral forms. It is feasible to use different discretization schemes within regions adjacent to either side of the coupling slots. In the simulation of the T-junctions, the circular waveguide is discretized with orthogonal grids conformal to the cylindrical coordinate system. This way, grids automatically match the cylindrical metal boundaries of the circular waveguide. The agreement between fitted and simulated results is excellent. Also, satisfactory agreement between the model and measurements is noted. The ripple and frequency shift present in the measured data are attributed mainly to the two coaxial line-to-rectangular waveguide transitions that were added at ports 1 and 2 for measurement purposes. The measured

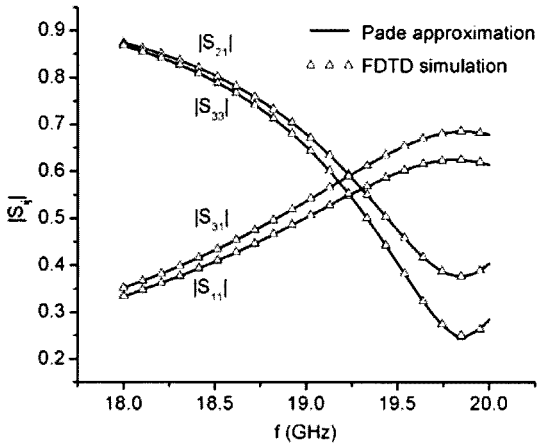

(a)

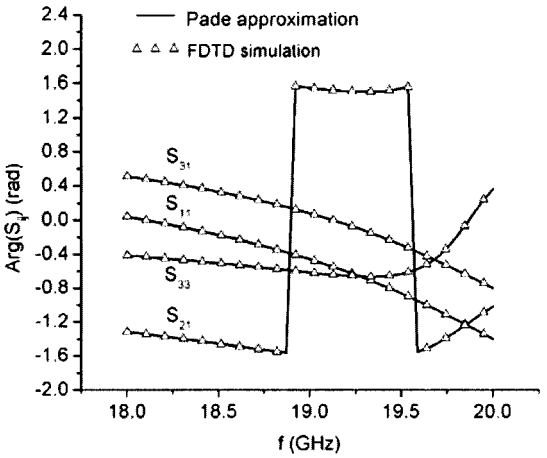

(b)

Fig. 8. Comparison of modeled and simulated S_{11}, S_{21}, S_{31} and S_{33}. $w = 6.5$ mm, $l = 1.5$ mm. (a) Amplitude. (b) Phase.

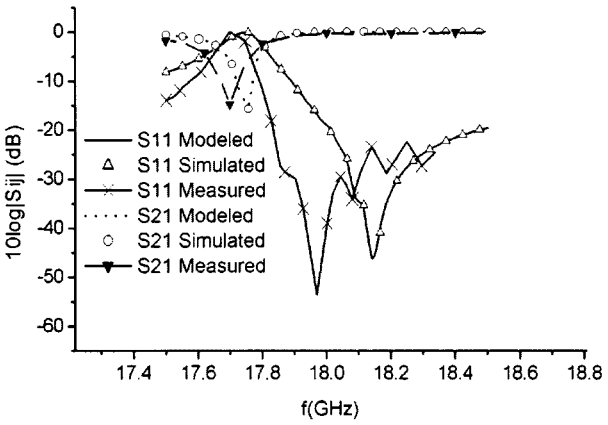

Fig. 9. Modeled, simulated and measured S_{11} and S_{21} when port 3 is short-circuited, for the case: $w = 6.1$ mm, $l = 1.3$ mm, $d = 10$ mm.

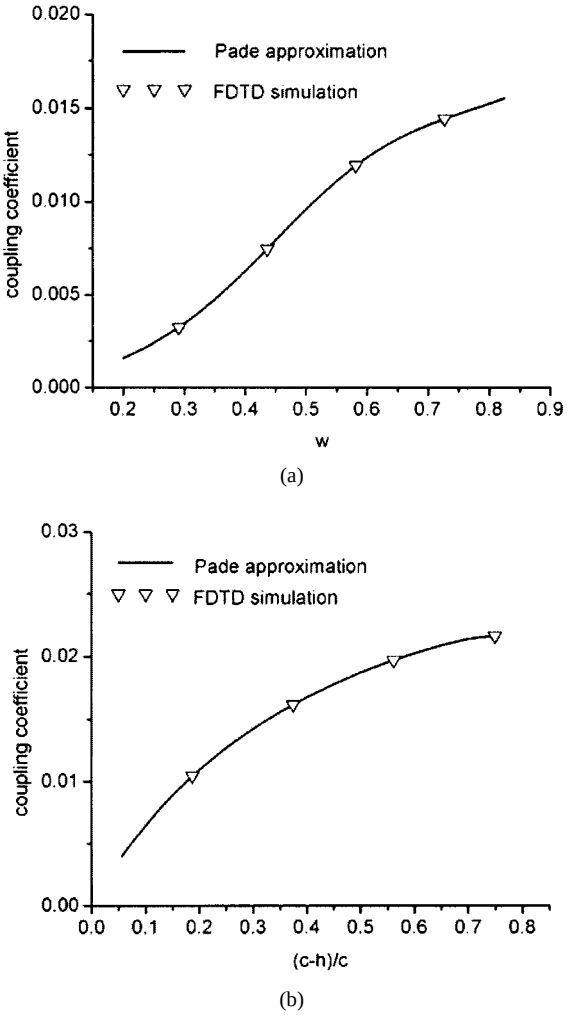

Fig. 10. Comparison of FDTD simulated and Pade modeled coupling coefficients for the case where magnetic coupling is dominant. (a) Dependence on slot width ($h = 0.951$ mm). (b) Dependence on slot height ($w = 2.22$ mm). $a = 2.22$ mm, $b = 2.54$ mm, $c = 4.75$ mm, $R = 0.33$ mm, $d = 3.76$ mm, $t = 0.132$ mm.

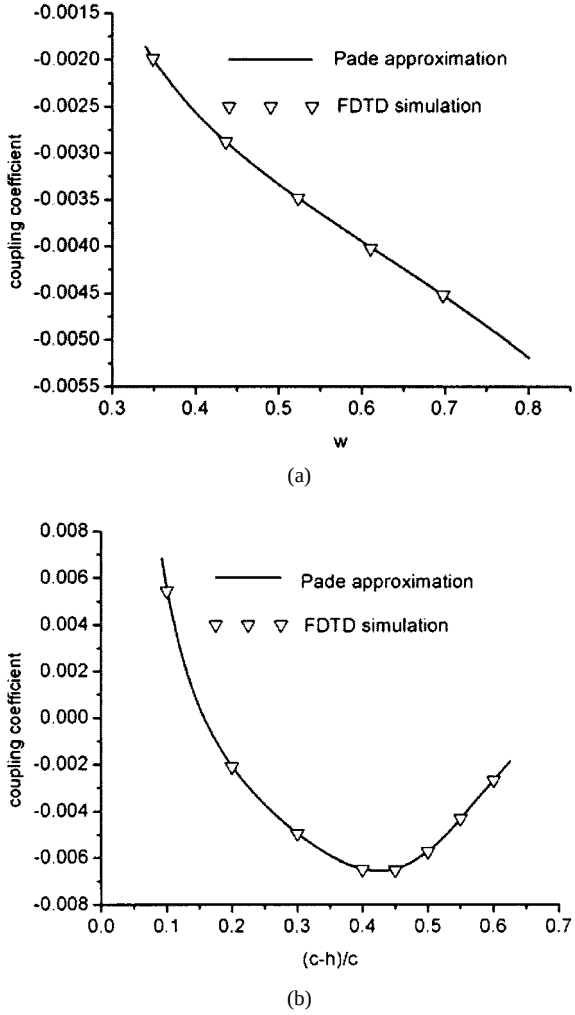

Fig. 11. Comparison of FDTD simulated and Pade modeled coupling coefficients for the case where electric coupling is dominant. (a) Dependence on slot width ($h = 2.38$ mm). (b) Dependence on slot height ($w = 2.22$ mm). The other parameters are the same as Fig. 10.

data shown in Fig. 9 included the effects of these two transitions; however, the FDTD simulations did not include them.

B. Coupling Slot in Rectangular Resonators

Computationally efficient CAD of combline filters requires the coupling coefficient of the slot to be available as an explicit function of the frequency and structural parameters that impact and control its value. For example, for the filters composed of the structures shown in Fig. 1, M_{ij} must be explicitly expressible as a function of the width and height of the coupling slot. Figs. 10 and 11 depict the dependence of the coupling coefficient on slot width and slot height. Furthermore, a comparison is provided between the simulated coupling coefficients from a brute-force FDTD simulation with the result obtained from the generated rational function approximation, for the cases of electric and magnetic coupling, respectively. For electric coupling, the slot is located near the open-circuited end of the resonator, while for magnetic coupling the slot is placed near the short-circuited end of the resonator.

C. Design of Combline Filters

As an engineering application of the proposed modeling and fitting methodologies, the design of two six-pole combline filters for wireless communication base station was undertaken. The slot and resonator configuration for the filters is shown in Fig. 12. The corresponding circuit topology is shown in Fig. 13, where the electromagnetic couplings introduced by the slots between resonators 1 and 4 and between resonators 3 and 6 create the transmission zeros at the stop band. The center frequency for design 1 is 900 MHz with a bandwidth of 20 MHz. For design 2, the center frequency is 1800 MHz with a bandwidth of 20 MHz. The normalized input/output resistances and coupling matrices for the filters are obtained from a two-step procedure as follows.

Since elliptic-like function filters have no explicit expression for their zeros and poles, an additional algorithm is needed to determine the zeros and poles for a given specification. The basic idea is to calculate the values of the characteristic function and its first-order derivatives at the zeros, poles, and the cutoff frequency ω_s, and then, through an adaptive simulated annealing optimiza-

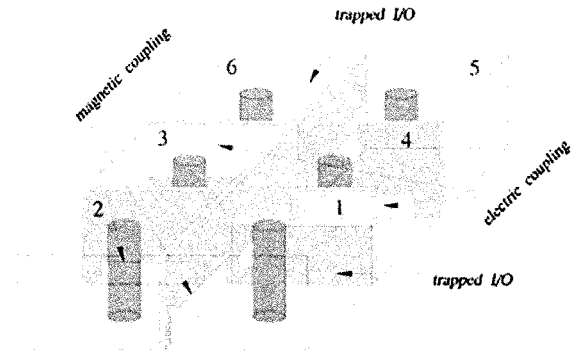

Fig. 12. Resonator and slot configuration for the six-pole combline filters.

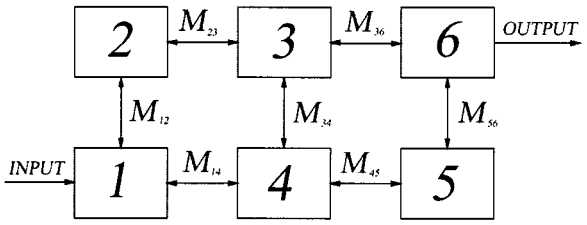

Fig. 13. Circuit topology for the six-pole filters shown in Fig. 12.

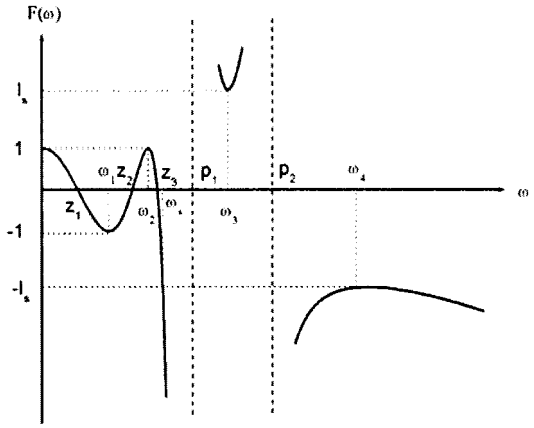

Fig. 14. Plot of the characteristic function $F(\omega)$.

TABLE I
DIMENSIONS OF THE RESONATORS (UNITS: MILLIMETERS)

	resonator length a	resonator width b	resonator height c	inner rod radius R	inner rod height d
Design 1	4.43	5.08	9.51	0.66	7.51
Design 2	2.22	2.54	4.75	0.33	2.73

tion, obtain the zeros, poles, and the ripple factor. Specifically, the desirable response for the general case is written as

$$|S_{21}|^2 = \frac{1}{1+\varepsilon^2 F^2(\omega)} \tag{22}$$

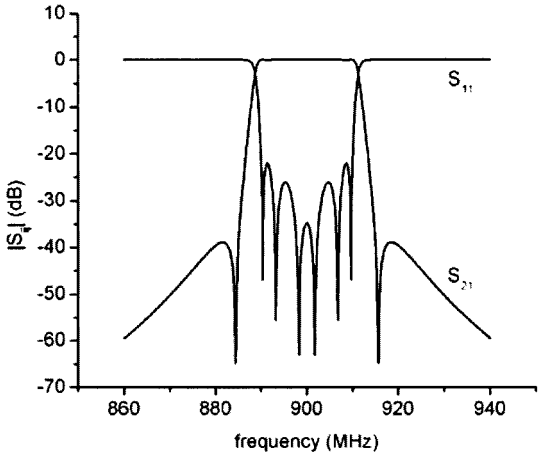

(a)

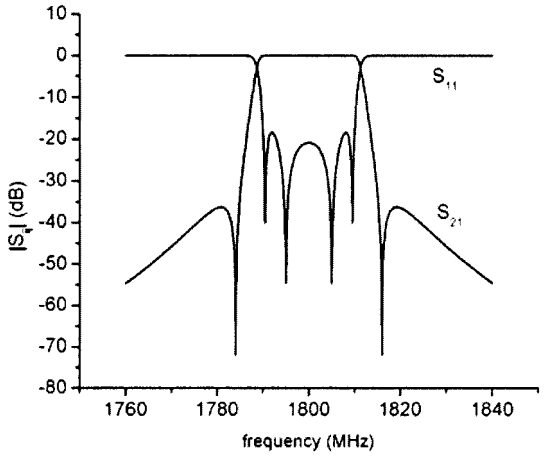

(b)

Fig. 15. Simulated frequency responses for the two combline filters. (a) Design 1 (900 MHz). (b) Design 2 (1800 MHz).

where ε is the ripple factor, and the characteristic function $F(\omega)$ reads

$$F(\omega) = C\omega^r \frac{\prod_{k=1}^{m}(\omega^2 - z_k^2)}{\prod_{k=1}^{l}(\omega^2 - p_k^2)},$$
$$|z_k| < 1,\ |p_k| > 1,\ r + 2m + 1 \geq 2l$$

where C is the normalized coefficient to be determined. For a six-pole filter, $F(\omega)$ can be written as

$$F(\omega) = C\frac{(\omega^2 - z_1^2)(\omega^2 - z_2^2)(\omega^2 - z_3^2)}{(\omega^2 - p_1^2)(\omega^2 - p_2^2)}. \tag{23}$$

Fig. 14 depicts $F(\omega)$ for a six-pole filter, where ten unknown parameters, including C, satisfy the following constraints:

$$\begin{aligned} &0 \leq z_1,\ z_2,\ z_3 < 1 \\ &1 \leq p_1,\ p_2 < 5 \\ &0 \leq \omega_1,\ \omega_2 < 1 \\ &1 \leq \omega_3,\ \omega_4 < 5. \end{aligned} \tag{24}$$

TABLE II
SIZES OF THE COUPLING SLOTS (UNITS: MILLIMETERS)

	1↔2		2↔3		3↔4		4↔5		5↔6		1↔4		3↔6	
	w	h	W	h	W	h	W	h	w	h	w	h	W	h
Design1	4.43	3.03	4.43	1.78	4.43	1.44	4.43	1.91	4.43	2.99	4.43	3.63	4.43	4.18
Design 2	2.22	0.43	1.04	0.95	2.22	1.79	2.22	0.54	2.22	1.99	2.22	0.95	2.22	0.53

Refering to Fig. 14, a simultaneous set of equations for $F(\omega)$ can be obtained as

$$\begin{aligned} F(\omega)|_{\omega=z_k} &= 0, \qquad k = 1, 2, 3 \\ F(\omega)|_{\omega=\omega_1} &= -1, \qquad F(\omega)|_{\omega=\omega_2} = 1, \\ F(\omega)|_{\omega=0} &= 1, \qquad F(\omega)|_{\omega=1} = -1, \\ F(\omega)|_{\omega=\omega_s} &= -I_s, \qquad F(\omega)|_{\omega=\omega_3} = I_s, \\ F(\omega)|_{\omega=\omega_4} &= -I_s, \\ \frac{\partial F(\omega)}{\partial \omega}|_{\omega=\omega_k} &= 0, \qquad k = 1, 2, 3, 4. \end{aligned} \tag{25}$$

From (22)–(25), the adaptive simulated annealing optimization is used to obtain the zeros, poles, and the ripple factor.

Once the zeros, poles, and the ripple factor have been determined, what remains is the determination of the optimized coupling matrix and input/output resistances according to the known circuit topology of the combline filter. Once again, adaptive simulated annealing optimization is used. The details of the algorithm can be found in [23] and [24].

Using this process, the normalized coupling matrix and input/output resistances are found to be as shown at the bottom of this page. The negative elements indicate that electric coupling is dominant. Accordingly, the slots should be located at the open-circuited end of the resonators. Positive elements indicate that magnetic coupling should be dominant. Thus, the slots must be located at the short-circuited end of the resonators. The coupling matrices given above are normalized. Thus, for determining the filter dimensions, these normalized coupling coefficients have to be multiplied by f_0/B_W, where f_0 and B_W represent the center frequency and the bandwidth of the filter, respectively.

The structural parameters of the filters that realize the coupling coefficients m_{ij} are obtained from the rational approximation model generated from FDTD simulations. Table I gives the dimensions of the resonators in the filters, while Table II gives the sizes of the coupling slots. The slot thickness is 0.132 mm for Design 1 and 0.066 mm for Design 2. Fig. 15(a) and (b) presents the simulated frequency responses of the two filters.

VI. CONCLUSION

A novel methodology for the efficient and accurate FDTD simulation of slot-coupled microwave structures has been presented. The present implementation is a hybridization of FDTD and the Padé approximation technique. It eliminates the need for subgridding, thus facilitating modeling versatility, avoiding numerical stability problems and improving computational efficiency. The proposed methodology is also applicable to the FDTD-based modeling of multilayered, slot-coupled printed antennas and 3-D MCM interconnects with perforated ground planes. Moreover, a methodology has been presented for the construction of closed-form expressions for the electromagnetic responses from FDTD-generated data. The methodology is based on an extension of the complex matrix valued multivariable Padé approximation. Availability of such closed-form expressions facilitates the expedient computer-aided design of microwave components. The proposed methodologies were validated through comparisons with measurements. Furthermore, their application to the design of combline filters was demonstrated.

$$M_1 = \begin{bmatrix} 0 & 1.054203 & 0 & -0.068507 & 0 & 0 \\ 1.054203 & 0 & 0.687714 & 0 & 0 & 0 \\ 0 & 0.687714 & 0 & 0.567333 & 0 & -0.150337 \\ -0.068507 & 0 & 0.567333 & 0 & 0.731909 & 0 \\ 0 & 0 & 0 & 0.731909 & 0 & 1.044080 \\ 0 & 0 & -0.150337 & 0 & 1.044080 & 0 \end{bmatrix}, \quad \text{for 900 MHz}$$

$$R_{01} = R_{67} = 1.746957$$

$$M_2 = \begin{bmatrix} 0 & 0.881238 & 0 & 0.588909 & 0 & 0 \\ 0.881238 & 0 & 0.490060 & 0 & 0 & 0 \\ 0 & 0.490060 & 0 & -0.172816 & 0 & 1.016223 \\ 0.588909 & 0 & -0.172816 & 0 & 1.032956 & 0 \\ 0 & 0 & 0 & 1.032956 & 0 & -0.292021 \\ 0 & 0 & 1.016223 & 0 & -0.292021 & 0 \end{bmatrix}, \quad \text{for 1800 MHz}$$

$$R_{01} = R_{67} = 1.232752$$

REFERENCES

[1] A. E. Atia and A. E. Williams, "Narrow bandpass waveguide filters," *IEEE Trans. Microwave Theory Tech.*, vol. MTT-20, pp. 258–265, Apr. 1972.

[2] H. W. Yao, K. A. Zaki, A. E. Atia, and R. Hershtig, "Full wave modeling of conducting posts in rectangular waveguides and its application to slot coupled combline filters," *IEEE Trans. Microwave Theory Tech.*, vol. MTT-43, pp. 2824–2830, Dec. 1995.

[3] Y. Rong and K. A. Zaki, "Full-wave analysis of couplings between cylindrical combline resonators," *IEEE Trans. Microwave Theory Tech.*, vol. 47, pp. 1721–1729, Sept., 1999.

[4] M. K. Montrose, *EMC and the Printed Circuit Board: Design, Theory and Layout Made Simple*. Piscataway, NJ: IEEE Press, 1996.

[5] M. Yamamoto and K. Itoh, "Behavior of the parallel plate mode in a stripline slot-coupled patch antenna," *Proc. Inst. Elect. Eng.*, vol. 147, pp. 385–389, 2000.

[6] L. Hyvonen, L. Hujanen, and A. Hujanen, "A compact MMIC-compatible microstrip to waveguide transition," in *IEEE MTT-S Int. Microwave Symp. Dig.*, 1996, pp. 875–878.

[7] A. Taflove, *Computational Electrodynamics: The Finite-Difference Time-Domain Method*. Norwood, MA: Artech House, 1995.

[8] R. Lotz, J. Ritter, and F. Arndt, "Locally conformed subgrid FD-TD technique for the analysis of 3D waveguide structures with curved metallic objects," in *IEEE MTT-S Int. Microwave Symp. Dig.*, 1999, pp. 1277–1280.

[9] I. S. Kim, "A local mesh refinement algorithm for the time domain finite difference method using Maxwell's curl equations," *IEEE Trans. Microwave Theory Tech.*, vol. 38, pp. 812–815, June 1990.

[10] S. Dey and R. Mittra, "A locally conformed finite-difference time-domain (FD-TD) algorithm for modeling three-dimensional perfectly conducting objects," *IEEE Trans. Microwave Guided Wave Lett*, vol. 7, pp. 273–275, Feb. 1997.

[11] S. Kapoor, "Sub-cellular technique for finite-difference time-domain method," *IEEE Trans. Microwave Theory Tech.*, vol. 45, pp. 673–677, May 1997.

[12] K. S. Yee and J. S. Chen, "The finite-difference time-domain (FDTD) and the finite-volume time-domain (FVTD) methods in solving Maxwell's equations," *IEEE Trans. Antennas Propagat.*, vol. 45, pp. 354–363, Mar. 1997.

[13] P. R. Graves-Morris, "Vector valued rational interpolants I," *Numer. Math.*, vol. 42, pp. 331–348, 1983.

[14] ——, "Vector-valued rational interpolants II," *SIMA J. Numer. Anal.*, vol. 4, pp. 209–224, 1984.

[15] R. E. Collin, *Field Theory of Guided Waves*. New York: IEEE Press, 1991.

[16] G. Conciauro, M. Guglielmi, and R. Sorrentino, *Advanced Modal Analysis: CAD Techniques for Waveguide Components and Filters*. New York: Wiley, 1999.

[17] G. A. Baker, Jr. and P. R. Graves-Morris, *Padé Approximants*. Cambridge, U.K.: Cambridge Univ. Press, 1996.

[18] R. Vich, *Z Transform Theory and Applications*. Boston, MA: D. Reidel, 1987.

[19] J. A. Pereda, F. Alimenti, P. Mezzanotte, L. Roselli, and R. Sorrentino, "A new algorithm for the incorporation of arbitrary linear lumped networks into FDTD simulations," *IEEE Trans. Microwave Theory Tech.*, vol. 47, pp. 943–949, July, 1998.

[20] S. F. Peik, R. R. Mansour, and Y. L. Chow, "Multidimensional Cauchy method and adaptive sampling for an accurate microwave circuit modeling," *IEEE Trans. Microwave Theory Tech.*, vol. 46, pp. 2364–2731, Dec., 1998.

[21] R. S. Adve, T. K. Sarkar, S. M. Rao, E. K. Miller, and D. R. Pflug, "Application of the cauchy method for extrapolating/Interpolating narrow-band system responses," *IEEE Trans. Microwave Theory Tech.*, vol. 45, pp. 837–845, May 1997.

[22] J. Cao, A. S. Rong, H. X. Wang, and X. H. Chen, "Determination of optimum conductivity profile for PML and PML-D using multiple-variables Pade approximation," in *IEEE MTT-S Int. Microwave Symp. Dig.*, 2000, pp. 1133–1136.

[23] W. A. Atia, K. A. Zaki, and A. E. Atia, "Synthesis of general topology multiple coupled resonator filters by optimization," in *IEEE MTT-S Int. Microwave Symp. Dig.*, 1998, pp. 821–824.

[24] L. O. Chua and P. M. Lin, *Computer-Aided Analysis of Electronic Circuits*. Englewood Cliffs, NJ: Prentice-Hall, 1975.

Ao Sheng Rong (M'96) received the B.S. and M.S. degrees in electronics engineering and the Ph.D. degree in radio engineering from the Southeast University (SEU), Nanjing, China, in 1982, 1984 and 1988, respectively.

In May 1988, he joined the faculty of the Department of Radio Engineering, Southeast University, where he is currently a Professor. He is also with the State Key Laboratory of Millimeter Waves, SEU. While on leave from SEU, he was a Visiting Scholar at the Oregon State University from 1994 to 1995. Since November 2000, he has been a Visiting Research Professor at the University of Illinois at Urbana-Champaign. His current research interests are in frequency- and time-domain electromagnetic simulations of interconnects and electronic packages, the characterization and design of RF/microwave/millimeter-wave integrated circuits and components, printed circuit antennas, and interactions of electromagnetic waves with inhomogeneous media. He has authored or co-authored over 80 technical papers. He is currently on the Editorial Board for the *Journal of Southeast University*.

Dr. Rong is a senior member of the Chinese Institute of Electronics (CIE). He was the recipient of the National Natural Science Prize, China, in 1991.

Heng Yang, photograph and biography not available at the time of publication.

Xing Hao Chen, photograph and biography not available at the time of publication.

Andreas Cangellaris (M'86–SM'97–F'00) received the Diploma degree in electrical engineering from the University of Thesalloniki, Thesalloniki, Greece, in 1981, and the M.S. and Ph.D. degrees in electrical engineering from the University of California at Berkeley, in 1983 and 1985, respectively.

He is currently a Professor of electrical and computer engineering at the University of Illinois at Urbana-Champaign. Prior to joining the University of Illinois at Urbana-Champaign in 1997, he was with the faculty of the Department of Electrical and Computer Engineering, University of Arizona, from 1987 to 1997. After finishing his doctoral studies, and from 1985 to 1987, he was a Senior Eesearch Engineer in the Department of Electronics Engineering, General Motors Research Laboratories, Warren, MI. His research interests and contributions are in two major areas. The first is the area of applied computational electromagnetics. The second is the area of modeling and simulation for high-speed interconnection and package electrical analysis. He has authored and co-authored over 100 scientific journal and conference papers in these areas.

Prof. Cangellaris is co-founder of the IEEE Topical Meeting on Electrical Performance of Electronic Packaging, which is sponsored jointly by the IEEE Microwave Theory and Techniques Society (IEEE MTT-S) and the IEEE Components, Packaging and Manufacturing Technology Society. He served as the meeting co-chair for the first three years. Since then, he serves as a member of its Technical Program Committee. Today, this meeting is considered the premier conference on package electrical analysis and design. He is also an active participant in the Electronic Components and Technology Conference (ECTC), as a member of the Technical Program Subcommittee on Modeling and Simulation. In addition, he serves as member of the Technical Program Committee for the IEEE MTT-S International Microwave Symposium. In 1998, he was the general chairman for the 8th Biennial Conference on Electromagnetic Field Computation, Tucson, AZ, which is sponsored by the IEEE Magnetics Society.